CONTINUUM MODEL SIMULATIONS AND EXPERIMENTS OF PROJECTILE IMPACT ON WOVEN FABRIC

Ethan M. Parsons* and Simona Socrate
Massachusetts Institute of Technology
Cambridge, MA 02139

Tusit Weerasooriya
U.S. Army Research Laboratory
Aberdeen Proving Ground, MD 21005-5069

Sai Sarva
General Electric Global Research
Niskayuna, NY 12309

ABSTRACT

Modeling woven fabrics is challenging due to the need to capture the fabric response at both the macroscopic scale of the fabric and the "mesoscale" of the yarns that compose the weave. Here, we utilize a continuum-level modeling technique for woven fabrics (King et al., 2005) which captures the macroscopic response of the fabric as well as the evolution of its mesostructure with deformation in a single efficient modeling step. A membrane element formulation of the model is implemented into a nonlinear finite element code ("Adlib", Deiterding et al., 2006) with a fully explicit solver and hard contact. In addition to displacement degrees of freedom, degrees of freedom representing the crimp amplitude of each yarn family are defined in order to solve for the configuration of the fabric unit cell at each step in time. The accuracy of the model is verified by comparing the simulation results with the experiments of Weerasooriya et al. (2008).

1 INTRODUCTION

Starting in the 1950's with vests constructed from ballistic nylon, fabrics woven from high strength fibers have been crucial to the safety of military personnel. The most well-known application of woven fabrics is lightweight, flexible body armor for protection against bullets and fragmenting projectiles from sources such as grenades, mortars, mines, and IED's. Woven fabrics are also used to reinforce polymers or ceramics in helmets and armor panels for protection against high-velocity projectiles. Additional common uses include restraint systems such as seat belts and head restraints, deployable fabric structures including air bags and air beams, as well as other forms of ballistic protection such as pilot seats. Most recently, fabrics are being utilized to increase the portability and durability of personal electronic devices.

Despite decades of research, the design of woven fabric systems is still largely based on empirical methods and experience. Modeling woven fabrics is challenging due to the need to capture the fabric response at both the macroscopic scale of the fabric and the "mesoscale" of the yarns that compose the weave. In fact, there is no widely accepted computational model for fabric deformation which is both computationally efficient and able to represent the behavior and evolving structure of the fabric at the level of the individual yarns. In the literature, either the fabric has been modeled at the level of the mesoscale, with detailed discretization of each fiber in the weave, or the fabric has been modeled at the continuum level, with phenomenological approaches, typically treating the fabric as an anisotropic continuum with two preferred material directions. In the first approach, the discretization length scale is determined by the dimensions of the fibers and weave, and thus real-sized or multi-ply simulations are computationally prohibitive. The second approach cannot be used to design fabrics based on the properties of the fibers and weave, and it is unsuitable for applications where the macroscopic response depends on the fabric's unique underlying mesostructure and its specific deformation mechanisms, such as fiber failure, crimp interchange, shear locking, or relative slip between the two fiber families. As such, without suitable models, the analysis and improvement of existing products and the development of new applications for woven fabrics is currently overly costly and time consuming.

Here, we utilize a continuum-level modeling technique for woven fabrics (King et al., 2005) which captures the

Report Documentation Page

Form Approved
OMB No. 0704-0188

1. REPORT DATE	2. REPORT TYPE	3. DATES COVERED
DEC 2008	**N/A**	**-**

4. TITLE AND SUBTITLE	5a. CONTRACT NUMBER
Continuum Model Simulations And Experiments Of Projectile Impact On Woven Fabric	5b. GRANT NUMBER
	5c. PROGRAM ELEMENT NUMBER
6. AUTHOR(S)	5d. PROJECT NUMBER
	5e. TASK NUMBER
	5f. WORK UNIT NUMBER
7. PERFORMING ORGANIZATION NAME(S) AND ADDRESS(ES) **Massachusetts Institute of Technology Cambridge, MA 02139**	8. PERFORMING ORGANIZATION REPORT NUMBER
9. SPONSORING/MONITORING AGENCY NAME(S) AND ADDRESS(ES)	10. SPONSOR/MONITOR'S ACRONYM(S)
	11. SPONSOR/MONITOR'S REPORT NUMBER(S)

12. DISTRIBUTION/AVAILABILITY STATEMENT
Approved for public release, distribution unlimited

13. SUPPLEMENTARY NOTES
See also ADM002187. Proceedings of the Army Science Conference (26th) Held in Orlando, Florida on 1-4 December 2008, The original document contains color images.

14. ABSTRACT

15. SUBJECT TERMS

16. SECURITY CLASSIFICATION OF:			17. LIMITATION OF ABSTRACT	18. NUMBER OF PAGES	19a. NAME OF RESPONSIBLE PERSON
a. REPORT **unclassified**	b. ABSTRACT **unclassified**	c. THIS PAGE **unclassified**	**UU**	**8**	

macroscopic response of the fabric as well as the evolution of its mesostructure with deformation in a single efficient modeling step. An appropriate unit cell approximation, based on a pin-joined truss geometry, represents the weave architecture. The configuration of the unit cell is determined by the macroscopic deformation gradient and the satisfaction of local equilibrium. The forces on the unit cell, and in turn the corresponding continuum-level stresses, are calculated from physically motivated constitutive relations.

The fabric model is used to simulate projectile impact on single plies of plain-weave Kevlar. Direct comparisons are made with experimental data obtained from digital image correlation (DIC).

2 FABRIC MODEL

The woven fabric model of King et al. (2005) has been modified and extended in order to function efficiently within an explicitly integrated finite element framework ("Adlib", Deiterding et al., 2006).

2.1 Constitutive Model

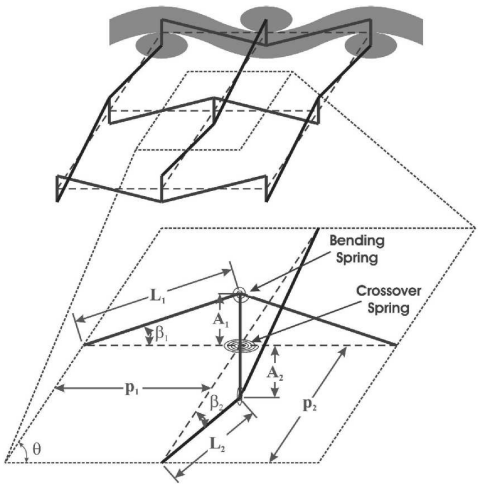

Figure 1: Geometry of fabric unit cell (King et al., 2006).

The fundamental basis of the model is the assumed unit cell geometry of the fabric shown in Figure 1. The unit cell approximates the mesoscale mechanisms of deformation that underlie the macroscopic response of the fabric. The continuum response at each material point along the fabric surface is obtained through homogenization of the unit cell response, which is in turn calculated through the *analytical* model described below. The warp ($k = 1$) and weft ($k = 2$) yarns are approximated as pin-joined, elastic trusses with the following properties:

p_k yarn quarter-wavelength
L_k yarn half-length or simply "length"

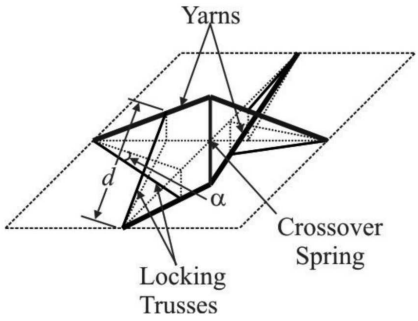

Figure 2: Geometry of fabric unit cell with locking spars (King et al., 2006).

β_k yarn crimp angle
A_k yarn crimp amplitude
θ in-plane angle between yarns

The torsional bending spring provides the resistance to bending of the yarns while the cross-over spring provides, at the cross-over points, torsional resistance to in-plane shear as well as compressive resistance to compaction of the yarns. Figure 2 illustrates the locking trusses of length d_k and angle α_k from the plane of the fabric which resist both shear and cross locking of the yarns. Constitutive relations describe each mode of deformation of the yarns. They are (with superscript "0" indicating an initial, undeformed value):

1. *extension*
   yarn tension, $T_k = k_k(L_k - L_k^0)$
2. *bending*
   bending moment, $M_{bk} = k_{bk}(\beta_k - \beta_k^0)$
3. *compaction*
   force in cross-over spring, $F_I = K_I(e^{aI} - 1)$, where $I = -\Delta A_1 - \Delta A_2$ is the interference of the yarns at the cross-over points.
4. *yarn locking*
   force in locking truss,
   $$F_{Lk} = \begin{cases} 0 & d_k^0 - d_k \le 0 \\ K_d(d_k^0 - d_k)^c & d_k^0 - d_k > 0 \end{cases}$$
5. *in-plane shear*
   moment, $M_s = K_s\gamma^e$, where the total relative yarn rotation, $\gamma = \theta^0 - \theta$, is separated into elastic and dissipative components, $\gamma = \gamma^e + \gamma^f$, which evolve according to $\dot{\gamma}_f = \dot{\gamma}_0 \left(\frac{M_s}{M_0}\right)$

k_k, k_{bk}, K_I, a, K_d, c, $\dot{\gamma}_0$, and M_0 are constants determined experimentally from simple experiments on single yarns and strips of fabric.

The deformed geometry of the unit cell in three dimensions is fully determined by the macroscopic deformation gradient, $\mathbf{F} = \text{Grad}\,\mathbf{x}(\mathbf{X}, t)$, and through-thickness equilibrium. $\mathbf{F}$ specifies the orientation and stretch of the

yarn vectors, $\mathbf{g}_1$ and $\mathbf{g}_2$, everywhere in the fabric:

$$\mathbf{g}_1 = \mathbf{F}\mathbf{g}_1^0 \quad \text{and} \quad \mathbf{g}_2 = \mathbf{F}\mathbf{g}_2^0. \tag{1}$$

p_1, p_2, and θ are calculated from $\mathbf{g}_1$ and $\mathbf{g}_2$. The out-of-plane state of the fabric (crimp amplitude) is derived from a force balance at the cross-over spring. At the end of each cross-over spring, for static equilibrium, the force in the cross-over spring, F_I, must balance the net through-thickness component of the force in the yarn trusses, F_k^N:

$$F_\mathrm{I} = F_k^\mathrm{N}, \ k = 1, 2. \tag{2}$$

F_I is given above, and F_k^N depends on the moments in the bending springs and the forces in the yarns and locking spars:

$$\begin{aligned} F_k^\mathrm{N} &= 2T_k \sin\beta_k - 2F_{\mathrm{L}l}\sin\alpha_l \left(1 + \frac{p_l|\cos\theta|\cos\beta_k}{L_k}\right) \\ &\quad + 2\left(\frac{k_{\mathrm{b}k}(\beta_k - \beta_k^0)}{L_k}\right)\cos\beta_k, \end{aligned} \tag{3}$$

where $l = 1, 2$ ($l \neq k$).

Finally, as illustrated schematically in Figure 3, in order to homogenize the mesoscopic, yarn-level forces to continuum-level stress measures, the stress on the unit cell must be computed. The first Piola-Kirchoff stress, $\mathbf{P} = \mathbf{P}(\mathbf{F}, \Delta A_1, \Delta A_2)$, is therefore calculated by equilibrating the external stress which must act on the loaded unit cell with the in-plane forces that the yarns exert on the unit cell.

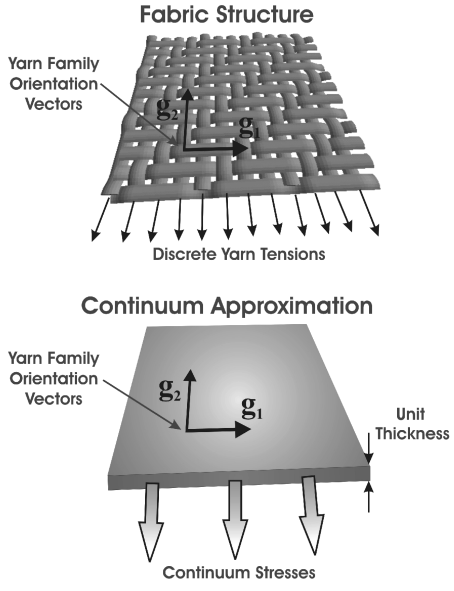

Figure 3: Modeling fabric as a homogeneous anisotropic continuum with current yarn directions $\mathbf{g_1}$ and $\mathbf{g_2}$ (King et al., 2006).

2.2 Finite Element Model

The fabric model has been integrated with the total Lagrangian framework of an explicit finite element code ("Adlib", Deiterding et al., 2006), in order to obtain a versatile tool for simulations of ballistic impacts on woven fabrics (WovenShield, Parasim Inc.). The degrees of freedom, $\mathbf{d}$, are the three components of macroscopic displacement, u_i, and the changes in yarn crimp amplitude, ΔA_1 and ΔA_2. The degrees of freedom are explicitly integrated forward in time via the Newmark method. At t^{n+1},

$$\mathbf{d}_{n+1} = \mathbf{d}_n + \Delta t \dot{\mathbf{d}}_n + \frac{\Delta t^2}{2}\ddot{\mathbf{d}}_n, \tag{4}$$

$$\ddot{\mathbf{d}}_{n+1} = \mathbf{M}^{-1}\left(\mathbf{f}_{n+1}^\mathrm{ext} + \mathbf{f}_{n+1}^\mathrm{int}\right), \tag{5}$$

and

$$\dot{\mathbf{d}}_{n+1} = \dot{\mathbf{d}}_n + \frac{\Delta t^2}{2}\left[\left(\ddot{\mathbf{d}}_n + \ddot{\mathbf{d}}_{n+1}\right)\right]. \tag{6}$$

The mass matrix, $\mathbf{M}$, is diagonal with the mass apportioned equally throughout the mesh.

The majority of resistance to ballistic impact loads is generated from in-plane deformation of the fabric and out-of-plane inertial effects. Out-of-plane bending and shear provide negligible contributions to the ballistic performance. As such, it was deemed sufficient to model the fabric as a membrane. 6-node triangular and 9-node rectangular elements were used.

The in-plane position of a material point in the reference configuration is given, as a function of the natural coordinates, ξ_s ($s = 1, 3$ for triangular elements; $s = 1, 2$ for rectangular elements) by the shape functions at each node, a:

$$X_J(\xi_s) = X_{Ja}N_a(\xi_s), \ J = 1, 2. \tag{7}$$

Correspondingly, the three-dimensional position of a material point in the current configuration is given by

$$x_i(\xi_s) = x_{ia}N_a(\xi_s), \ i = 1, 3. \tag{8}$$

The relevant components of the deformation gradient at a point within the element are therefore defined by

$$F_{iJ} = \frac{\partial x_i}{\partial X_J} = N_{a,J}x_{ia}. \tag{9}$$

Provided that the fabric initially lies in the 1-2 plane, $\mathbf{F}$ then determines the orientation and stretch of the yarn vectors, $\mathbf{g}_1$ and $\mathbf{g}_2$, at each integration point within the element. The internal nodal forces corresponding to the displacement degrees of freedom are then calculated by integrating numerically over the element:

$$(f_{ia}^\mathrm{int})^\mathrm{e} = -\int_{\Omega_0{}^\mathrm{e}} P_{iJ}(\mathbf{F})N_{a,J}\mathrm{d}V_0. \tag{10}$$

By virtual work considerations, multiplying Equation 2 by virtual changes in amplitude $\tilde{\Delta}A_k$ and integrating over the element provides the statement of equilibrium (excluding inertia and external forces) in weak

form:

$$\int_{\Omega_0{}^{\mathrm{e}}} \tilde{\Delta A}_k \frac{F_{\mathrm{I}}(\Delta A_1, \Delta A_2) - F_k^{\mathrm{N}}(\mathbf{F}, \Delta A_1, \Delta A_2)}{4p_1^0 p_2^0} \mathrm{d}S_0 = 0. \tag{11}$$

With $\Delta A_k(\xi_s) = \Delta A_{ka} N_a(\xi_s)$, the internal nodal forces corresponding to the amplitude degrees of freedom become

$$(f_{ka}^{\mathrm{int}})^{\mathrm{e}} = \int_{\Omega_0{}^{\mathrm{e}}} \frac{F_{\mathrm{I}}(\Delta A_1, \Delta A_2) - F_k^{\mathrm{N}}(\mathbf{F}, \Delta A_1, \Delta A_2)}{4p_1^0 p_2^0} N_a \mathrm{d}S_0. \tag{12}$$

The total mass of the element is given by

$$M = \rho_{\mathrm{f}} t_{\mathrm{f}} \frac{1}{2} W^q \sum_{q=1}^{3} J^q, \tag{13}$$

where ρ_{f} and t_{f} are the density and thickness, respectively, of the fabric and J^q and W^q are the Jacobian determinant and weight, respectively, at integration point q. In order to calculate the mass associated with the amplitude degrees of freedom, we take $L_1 \approx L_2 = L$, $\beta_1 \approx \beta_2 = \beta \equiv 0$ and $m_1 \approx m_2 = m \equiv M/4$. Moment equilibrium of a single half-length of yarn about its point of intersection with the unit cell boundary gives

$$Fl \approx I\ddot{\beta} = \frac{ml^2}{3}\ddot{\beta} = \frac{Ml^2}{12}\ddot{\beta}. \tag{14}$$

With the through-thickness acceleration of the free end approximated as $\ddot{A}_k \approx \ddot{\beta} l$, the through-thickness equilibrium equation becomes

$$F = \frac{M}{12}\ddot{A}_k. \tag{15}$$

Thus, when the mass of the other yarn half-length is included, we find that the lumped masses associated with the amplitude degrees of freedom are related to the corresponding masses associate with displacement degrees of freedom by a factor of $\frac{1}{6}$.

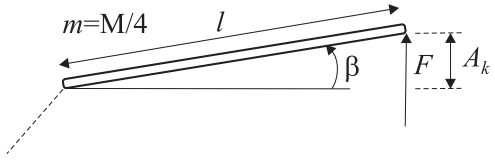

Figure 4: Calculation of lumped mass corresponding to amplitude degrees of freedom.

2.3 Quasi-Static Model Verification

In order to verify the accuracy of this new formulation of the fabric model, several standard test cases were simulated. In Figure 5, simulation results are compared with the experimental results of King et al. (2005) for uniaxial tension of 2.54 cm × 25.4 cm strips of fabric. The fabric tested by King et al., commonly known as S706, was 600 denier, plain-weave Kevlar KM2 with 34 threads per inch in both the warp and weft directions. All parameters used in the model were either measured by King et al. or fit to the experiments of King et al. 640 6-node planar triangular elements were used to model the strip. Excellent agreement is seen for loading in both the warp and weft directions.

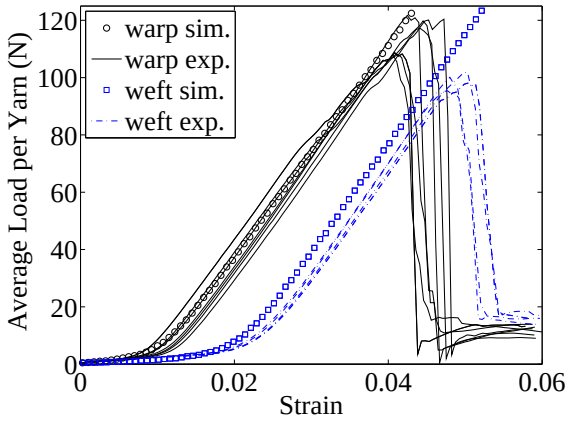

Figure 5: Simulations vs. experiments (King et al., 2005) for strips of Kevlar S706 under uniaxial tension in warp and weft directions.

Figure 6 plots simulation and experimental results for bias-extension. In this case, a 3.5 cm×9.5 cm strip of fabric, with the yarns aligned at 45° to the horizontal, was loaded in uniaxial tension. 300 6-node planar triangular elements were used to model the strip. The remarkable agreement between the simulation and experiments provides a validation of the ability of the model to simulate complex deformations.

3 EXPERIMENTAL PROCEDURE

Weerasooriya et al. (2008) conducted projectile impact experiments on single plies of the Kevlar S706. A gas gun was used to launch $d = 12.7$ mm hemispherically-nosed steel projectiles of mass 104 g at a striking velocity of 22 m/s. As shown in Figures 7 and 8, the approximately 40 cm square fabric specimens were stapled to 30.5 cm square "picture-frames" with a pneumatic staple gun. Frames with a 25.4 mm square cut-out and a $R = 12.7$ cm circular cut-out were used. The frames were clamped between two aluminum plates of similar dimensions. The surface of the aluminum plate in contact with the fabric was roughened in order to limit slipping of the fabric. The specimens were first painted with white spray paint, and then a speckle pattern was applied with black spray paint.

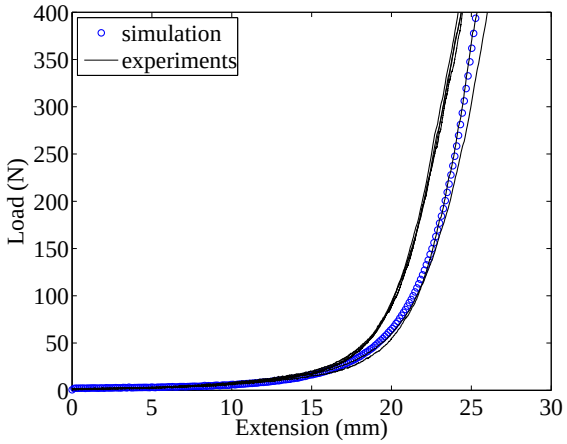

Figure 6: Simulation vs. experiments (King et al., 2005) for Kevlar S706 bias-extension test.

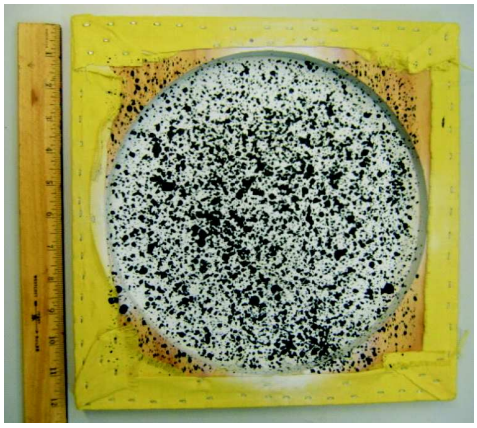

Figure 8: Back view of Kevlar fabric specimen stapled to frame with round hole.

Figure 9 illustrates the experimental set-up. The launch velocity of the projectile was measured at the outlet of the gun barrel with laser beam detectors. The detectors also triggered the two Photron APX-RS high speed digital cameras to start recording images. 256 × 256 pixel images of the back surface of the specimen were acquired at a rate of 30 kHz. Commercial digital image correlation software from Correlated Solutions, Inc. was then used to measure the full-field in-plane (u, v) and transverse (w) displacements of the fabric.

4 RESULTS

The fabric model was used to simulate the experiments of Weerasooriya et al. 2912 6-node triangular membrane elements and 900 9-node rectangular membrane elements, respectively, were used in the circular and square cases. Contact between the projectile and fabric was simulated as hard and without friction. While great care was taken in the experimental tests to minimize slip of the fabric from the clamps, as with nearly all experiments of this type, some slip did occur. For example, the DIC results for in-plane v-displacement in Figure 10 show that, during the $R = 12.7$ cm experiment, at least 4 mm of slip occurred from the clamps. On average, 3-5 mm of slip is apparent for both the square and circular tests. Therefore, in the simulations the edges of the specimen were not considered perfectly fixed at the clamps. Rather, a distributed frictional force consistent with the observed slip of the fabric was imposed on the perimeter of the fabric.

In Figures 11–14, the transverse displacements along lines in the warp and weft directions through the point of impact of the two fabrics are plotted for the experiments at four instances in time, with the final time correspond-

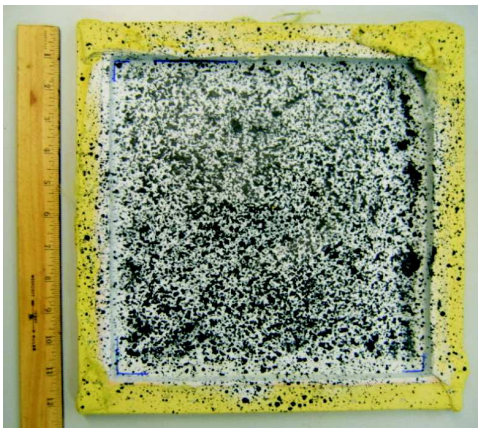

Figure 7: Front view of Kevlar fabric specimen stapled to frame with square hole.

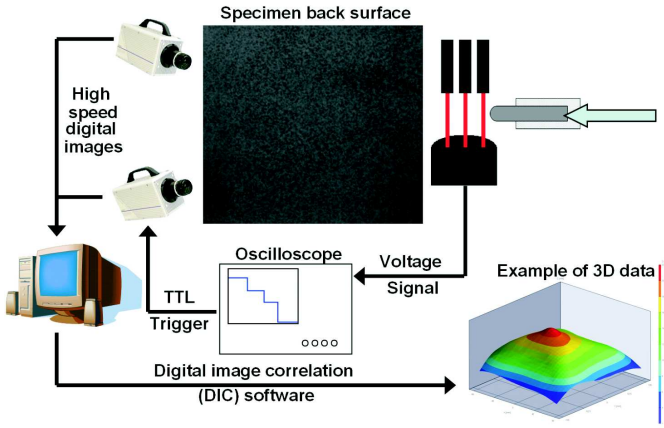

Figure 9: Schematic of experimental set-up for measuring full-field displacements during a ballistic impact test.

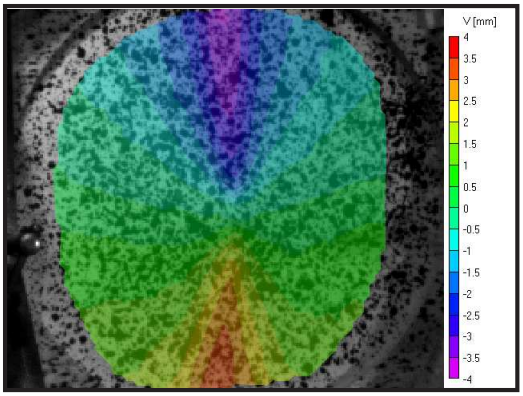

Figure 10: Contours of in-plane v-displacement during $R = 12.7$ cm experiment at $t = 2.0$ ms.

ing to the maximum displacement of the fabric. During the experiment, the fabric deforms almost identically in the warp and weft directions. The isotropy of the experimental results is an indication that the specimen is subject to a small prestretch. In fact, it is nearly impossible to clamp flat a fabric specimen without applying at least a small degree of preload. In the simulations, the effects of preload are accounted for by specifying an initial deformation gradient, $\mathbf{F}^{\text{pre}}$, and initial changes in yarn amplitude, ΔA_1^0 and ΔA_2^0. These parameters were determined by subjecting a single 4-node, reduced integration finite element to increasing levels of biaxial tension. Single element simulations were conducted with both equal force and equal strain in the warp and weft directions. A parametric study with varying levels of $\mathbf{F}^{\text{pre}}$ and ΔA_i^0 was conducted for the $R = 5$ inch simulations. It was found that a preload with equal force in

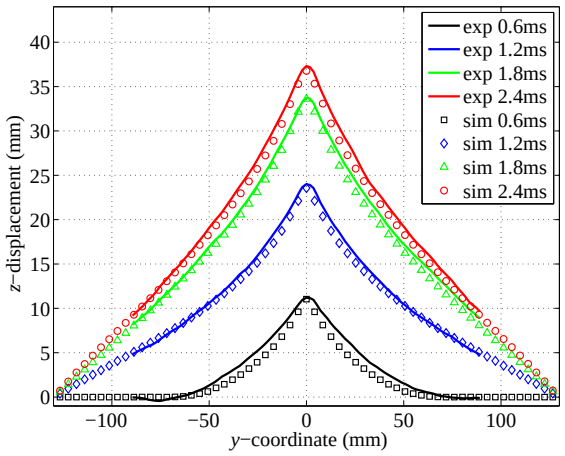

Figure 11: Experiment versus simulation of $R = 12.7$ cm fabric, clamped at circumference, for $v_{\text{i}} = 22$ m/s: warp yarn transverse displacement through point of impact.

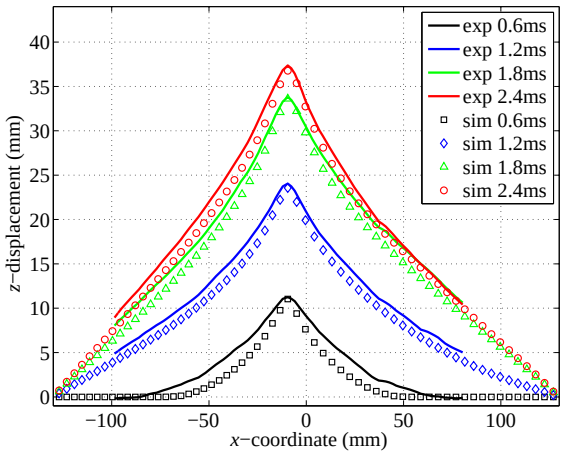

Figure 12: Experiment versus simulation of $R = 12.7$ cm fabric, clamped at circumference, for $v_{\text{i}} = 22$ m/s: weft yarn transverse displacement through point of impact.

the warp and weft directions provided a good fit to the experimental data. The preload was found to be 1.7 N per yarn, and the corresponding initial changes in amplitude were $\Delta A_1^0 = -0.013$ mm and $\Delta A_2^0 = -0.031$ mm. The results of the simulations with both fabric slip at the clamps and preload compared with the experiments are also plotted in Figures 11–14. Exceptional agreement between experiment and simulation is exhibited for both geometries of fabric specimen.

Figure 15 plots the history of displacement of the fabric at the point of impact for both the experiments and simulations. Overall, the simulations compare very well

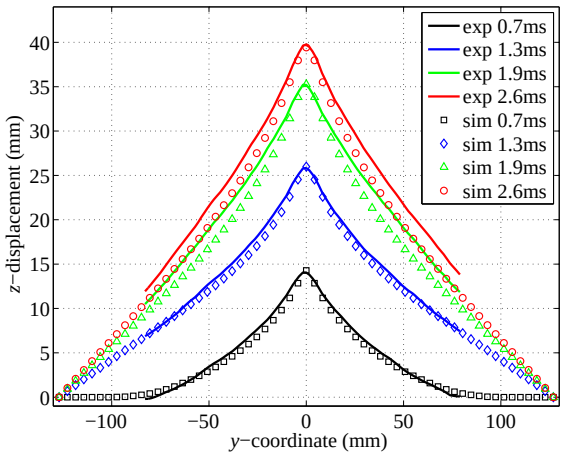

Figure 13: Experiment versus simulation of 25.4 cm square fabric, clamped on four sides, for $v_{\text{i}} = 22$ m/s: warp yarn transverse displacement through point of impact.

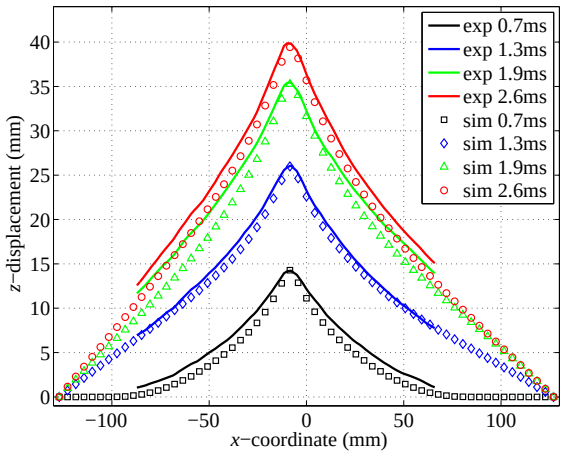

Figure 14: Experiment versus simulation of 25.4 cm square fabric, clamped on four sides, for $v_i = 22$ m/s: weft yarn transverse displacement through point of impact.

with the experiments, even during the rebound phase of the deformation. Figure 16 shows the deformed shape and contours of transverse displacement for the experiments and simulations with $R = 12.7$ cm. As expected from the previous results, there is an impressive correlation between the two. Furthermore, we note the "tent-like" deformation patterns of both the experiment and simulation. Observed by numerous experimentalists, this mode of deformation is due to the highly anisotropic properties of the fabric.

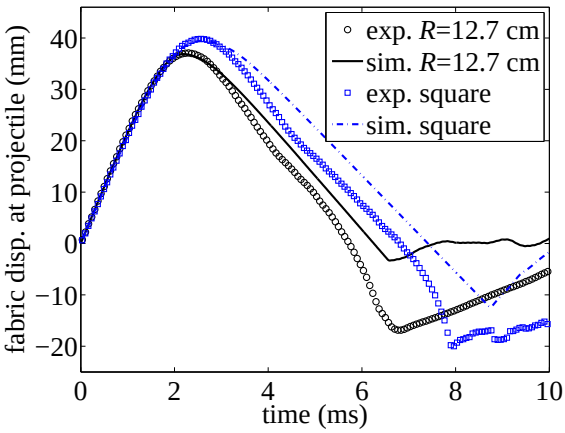

Figure 15: Experiment and simulation transverse displacement at point of impact for $v_i = 22$ m/s: $R = 12.7$ cm and 25.4 mm square.

5 CONCLUSIONS

The extension of the fabric model to an explicit finite element formulation with the deformed configuration of the unit cell determined solely from degrees of freedom driven by inertia has been a success. The model has proven to simulate projectile impact events accurately without excessive computational cost.

The model has many potential uses. Its computational efficiency enables the simulation of large and complex (including multi-ply) structures. Although a continuum-level model, it also simultaneously monitors the deformation of the fabric on the scale of individual yarns. Knowledge of local quantities such as yarn tension and yarn wavelength provides the ability to predict phenomenon such as penetration due to yarn breakage (e.g. bullet, knife threat) or yarn separation (puncture threat).

The framework of the model is versatile and may be applied to many existing or proposed materials. Other plain-weave Kevlar fabrics may be modeled by simply adjusting the purely physical material parameters. Fabrics of a different weave pattern require only a new unit cell geometry. Viscoelastic yarn deformation may be included in the model by modifying the tensile constitutive response of the yarns. Furthermore, its continuum nature will allow the model to be integrated with other material models for the simulation of fabric composites such as those used in helmets and armor panels.

ACKNOWLEDGEMENTS

This research was supported by the U.S. Army Research Office through the MIT Institute for Soldier Nanotechnologies under contract number W911NF-07-D-0004. The authors thank Professor R. Radovitzky for providing the explicit finite element framework, Adlib, in which we implemented the fabric model.

REFERENCES

Deiterding R., Radovitzky R., Mauch S.P., Noels L., Cummings J.C., and Meiron D.I., 2006: A Virtual Test Facility for the Efficient Simulation of Solid Material Response Under Strong Shock and Detonation Wave Loading, *Eng. Comp.*, **22**, 325-347.

King M., 2006: A Continuum Constitutive Model for the Mechanical Behavior of Woven Fabrics Including Slip and Failure, PhD Thesis, MIT, Cambridge, MA.

King M., Jearanaisilawong P., and Socrate S., 2005: A Continuum Constitutive Model for the Mechanical Behavior of Woven Fabrics, *Int. J. Sol. Struct.*, **42**, 3867-3896.

Weerasooriya T., Gunnarsson C.A., and Moy P.: Measurement of Full-Field Transient Deformation of the Back Surface of a Kevlar KM2 Fabric During Impact for Material Model Validation, *Proc. 2008 Int. Cong. Expos. Exp. Mech. Appl. Mech.*, June 2-5, Orlando, FL.

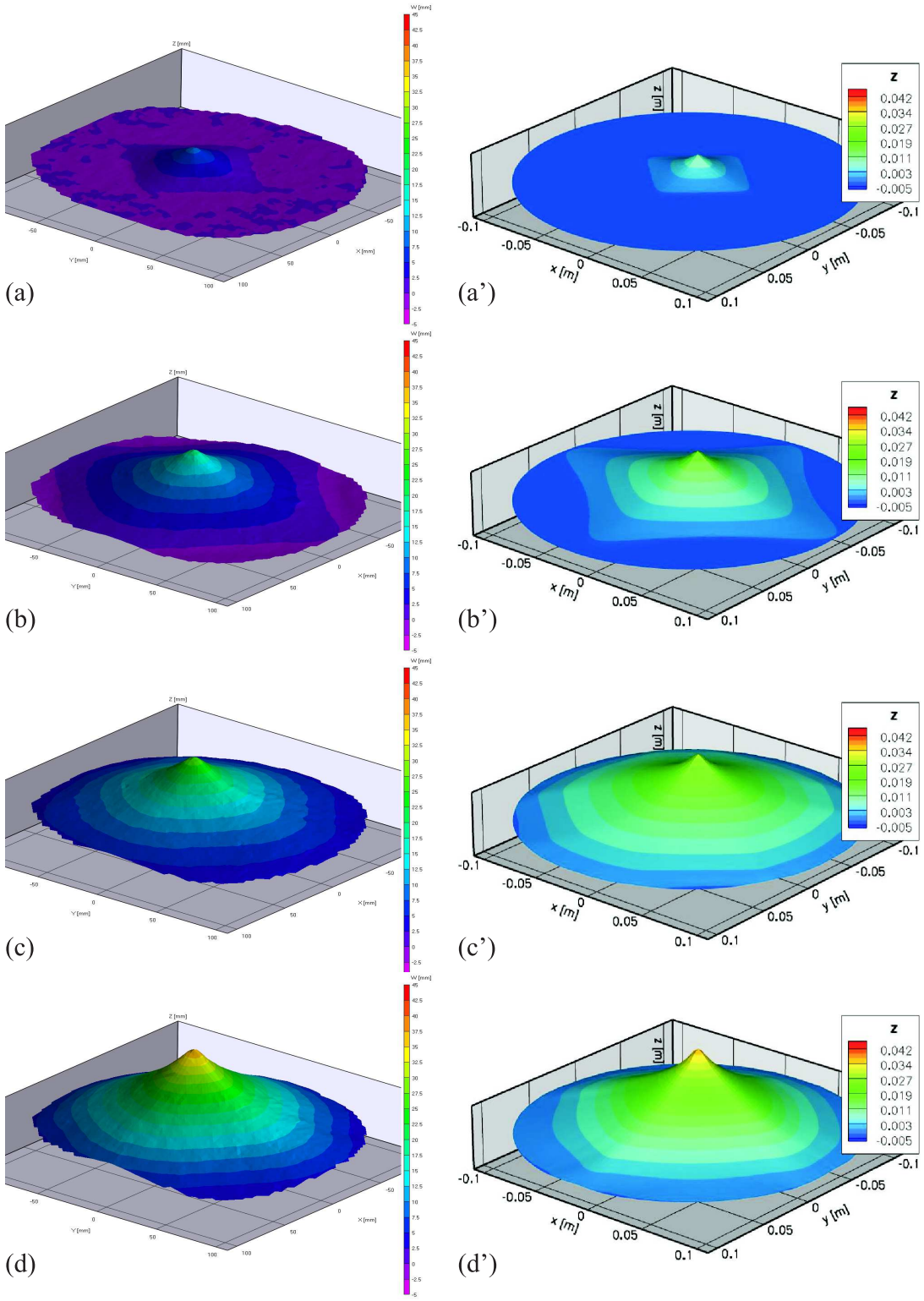

Figure 16: Contours of transverse displacement for experiment (left, in mm) and simulation (right, in m) for $R = 12.7$ cm fabric with $v_i = 22.2$ m/s as a function of time: (a), (a′) $t = 0.4$ ms; (b), (b′) $t = 0.9$ ms; (c), (c′) $t = 1.3$ ms; (d), (d′) $t = 2.0$ ms.